Journal of Materials Chemistry C

Accepted Manuscript

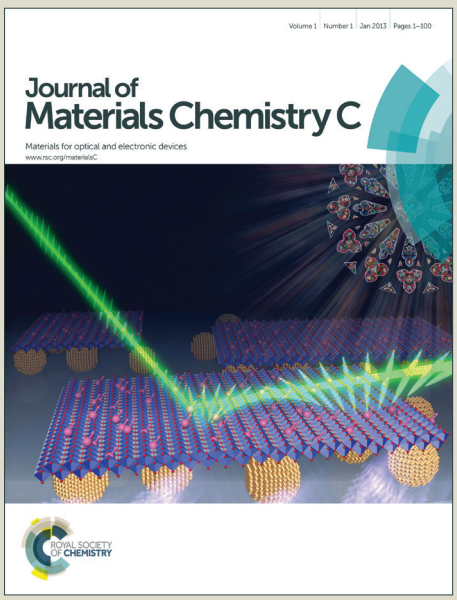

ROYAL SOCIETY OF CHEMISTRY

www.rsc.org/materialsC

Journal of Materials Chemistry C

RSCPublishing

Paper

Controlled synthesis and optimum luminescence of Sm^{3+} -activated nano/submicro ceria particles by a facile approach

Cite this: DOI: 10.1039/xoxxoooooox

Received ooth January 2013,
Accepted ooth January 2013

DOI: 10.1039/xoxxoooooox

www.rsc.org/

Jingjing Wu,[a] Shikao Shi,[*a] Xiaolong Wang,[a] Jibiao Li,[a] Ruilong Zong[b] and Wei Chen[c]

Rare-earth Sm^{3+} -activated nano/submicro ceria particles were prepared by a rapid combustion reaction. Characterized with X-ray diffraction patterns and Raman spectra, the formation of solid solution was confirmed after Sm^{3+} doping into ceria, and the concentration of oxygen vacancies in the host was gradually increased with the increase of Sm^{3+} doping content. Assisted by polyvinyl alcohol (PVA) in the combustion reaction process, the morphology of the particles was well-distributed and the particle size was controlled from nano (10 nm) to submicro (~250 nm), depending on the post- sintering temperature. The more interesting was that the samples could be effectively excited with 370 nm and emitted strong orange-red light after optimization, which was suitable for the demands of high-efficiency UV LEDs. Without the addition of PVA, the samples showed very weak luminescence even after a sintering duration. However, the samples prepared by PVA-assisted combustion synthesis exhibited remarkably enhanced emission after an appropriate heat-treatment. The quenching concentration of activator Sm^{3+} was 1.5 mol%, and the optimal luminescence intensity reached nearly 10-fold in comparison with that of samples prepared by conventional solid state reaction. The Sm^{3+} -activated nano/submicroscale ceria materials are potential for the use of solid state lighting.

1. Introduction

Ceria (CeO_2) is an important ceramic material due to its excellent properties such as superior thermal and chemical stability, high ionic conductivity, good oxygen storage or release capacity and strong UV absorption.[1] Recently, the investigation on rare-earth doped nanoceria has been given much attention in the fields of bio-medical and bio-imaging,[2-5] oxidation catalyst,[6,7] solid-oxide fuel cells[8,9] and ultraviolet shielding materials.[10] Among the rare-earth elements, Ce^{4+} and Sm^{3+} have close ionic radius and electronegativity, which is beneficial for the formation of Ce-Sm-O solid solution.[11] Yamashita et. al.[12] and Liu et al.[13] respectively reported that $Ce_{0.8}Sm_{0.2}O_{1.9}$ nanopowder prepared by hydrothermal and self-rising approach showed a higher conductivity value compared with traditional yttria-stabilized zirconia. Both Wang and Kuntaiah groups noticed that nanocrystalline $Ce_{0.6}Sm_{0.4}O_{1.8}$ synthesized through coprecipitation and hydrothermal process had better catalytic performance than pure ceria for the oxidation of CO.[7,11] However, the luminescence properties of Sm^{3+} -doped ceria were seldom mentioned owing to its very weak luminescence when prepared by traditional solid state reaction (SSR). Fujihara et al.[14] fabricated CeO_2:Sm^{3+} thin film and found a dominant magnetic-dipole $^4G_{5/2}\rightarrow{}^6H_{5/2}$ emission transition centered at 573 nm without the electric-dipole $^4G_{5/2}\rightarrow{}^6H_{9/2}$ transition.

Luminescence is one of the most important properties of rare-earth activated metal oxide nanoparticles.[15-18] Since the 4f electrons of trivalent rare-earth ions are well shielded from the surroundings, the emission transitions yield sharp lines in the spectra. Moreover, their 4f states only weakly interact with the host lattice, and therefore the energy differences are nearly constant, leading to almost the same light emission in different host lattice.[19] For example, Eu^{3+} as a popular activator, can generate intense red light which originates from the typical electric-dipole $^5D_0\rightarrow{}^7F_2$ transition in cubic Y_2O_3 and scheelite $CaWO_4$ hosts. However, the effective excitation wavelength is closely related with the structure. In cubic Y_2O_3: Eu^{3+}, the optimal excitation is from O-Y charge transfer (CT) band centered at about 240~260 nm,[20,21] which is quite suitable for the use of fluorescent lamps. Whereas, in scheelite $CaWO_4$:Eu^{3+} system, the most intense excitation is often from $^7F_0\rightarrow{}^5L_6$ (395 nm) transition of Eu^{3+}.[22,23]

Herein, we report a facile synthesis and luminescence properties of CeO_2 :Sm^{3+} nano/submicro particles prepared by a rapid PVA-assisted combustion synthesis (abbreviated as PVACS). The advantages of our work are based on the following three aspects. ① **A promising luminescence host because of obvious energy transfer from host to Sm^{3+}**. In contrast to rare-earth doped oxide phosphors such as Y_2O_3: Eu^{3+} and $CaWO_4$:Eu^{3+} system, rare-earth doped CeO_2 in view of luminescence has been relatively less studied.[14] The fact that Ce^{4+} ions have no 4f electron implies that CeO_2 can be a promising luminescence host material due to strong light absorption through CT from O-Ce. If the energy transfer is achieved from the CT state of CeO_2 to the doped rare-earth ions,

the characteristic emissions of rare-earth ions are expected to be observed. In the CeO_2: Sm^{3+} system, the evident CT band of $O^{2-}\rightarrow Ce^{4+}$ in the excitation spectrum was noticed by monitoring the emission of Sm^{3+}, which demonstrates the energy transfer from host to activator Sm^{3+}. ②**Controlled particle size and optimized luminescence**. Recently, we investigated Eu^{3+} -activated CeO_2 nanoparticles (60 nm) by simple combustion synthesis without the addition of PVA (abbreviated as SCS).[24] It was found that most crystallites had weak crystallinity and were not well-separated because of the instantaneous reaction. Even after a post-sintering process, the morphology and luminescence of the samples were hardly improved. To solve the problem, the surfactant PVA was added into the reactant solutions. After the combustion reaction, the particles showed well-dispersed and round shape, and the particle size was only about 10 nm. Moreover, the particle size and luminescence intensity of the samples could be readily controlled and optimized by a subsequent heat-treatment (from 600-900 ^oC) process. Therefore, the preparation by PVACS and post-sintering is simple, effective and practical.③**Potential application**. The as-prepared CeO_2:Sm^{3+} nano/submicro samples with strong luminescence may be suitable for the use of solid state lighting. It is known that one of the challenges for the UV LEDs is to develop stable, efficient, and environmental friendly phosphor that can be excited between 340 and 400 nm.[25-27] For CeO_2:Sm^{3+} nano/submicro particles, the effective excitation range is a CT band from 345 to 420 nm centered at 370 nm, which is expected to meet the demands of solid state lighting.

2. Experimental

2.1. Preparation of samples

A series of Sm^{3+} -doped ceria samples were prepared by PVACS. The raw materials contain $Ce(NO_3)_3{\cdot}6H_2O$ (Yongda Chemical, Tianjin, 99.5%), Sm_2O_3 (General Institute of Non-ferrous Metals, Beijing, 99.95%), urea (A.R.) and PVA (A.R.). All of them are used as-received without further purification. The Sm_2O_3 was first dissolved in nitric acid and formed $Sm(NO_3)_3$ aqueous solution. Then the rare-earth nitrate, urea and PVA were mixed according to the molar ratio of Ce: Sm: urea: PVA= (1-x): x: 5: 0.1. As the mixture was completely dissolved, the aqueous solution was continuously stirred for over 30 minutes, and put into a porcelain crucible to start a combustion reaction in a furnace (550 ^oC). After the rapid reaction process (only a few seconds), the samples were heat-treated in 600-900 ^oC for 2h. In addition, some samples prepared by SCS method were achieved. The similar preparation process and experimental phenomena on SCS have been described in previous report.[24]

For the convenience of comparison, the Sm^{3+} -doped ceria samples were also prepared by conventional SSR method. For this method, the initial materials CeO_2 (General Institute of Non-ferrous Metals, Beijing, 99.9%) and Sm_2O_3 were used, and the calcination temperature and duration time were 1000 ^oC and 2h, respectively.

2.2. Characterization

The X-ray diffraction (XRD) patterns of the samples were recorded on a D8 Advance X-ray powder diffractometer with CuKα (λ = 1.54056 Å) radiation (40 mA, 40 kV) employing a step size of 0.02° over a 2θ scan range of 25-80°. The Raman spectra were performed with a HORIBA JY HR800 confocal microscope Raman spectrometer using an Ar-ion laser (514.5 nm). The morphology and size of the as-prepared samples were characterized by an F-4800 field emission scanning electron microscopy (SEM). The Brunauer-Emmett-Teller (BET) specific surface area of the samples were examined by nitrogen adsorption/ desorption at 77K by using a Micromeritics 3020 analyzer. The emission and excitation spectra were measured on an F-4600 spectrofluorometer equipped with a Xe lamp, and both the emission and excitation slit width were 2.5 nm. The decay curves were recorded from Hamamatsu R928 photomultiplier as detector, YAG:Nd laser (355 nm), Acton Spectrapro-2300i spectrometer and Tektronix DPO4104 oscilloscope. The photoluminescence quantum yields of some samples were obtained using an HORIBA JOBIN YVON Nanolog FL-3-2iHR infrared fluorescence spectrometer with F-3018 integrating sphere. All the measurements were performed at room temperature.

3. Results and discussion

3.1 Structure and morphology characteristics

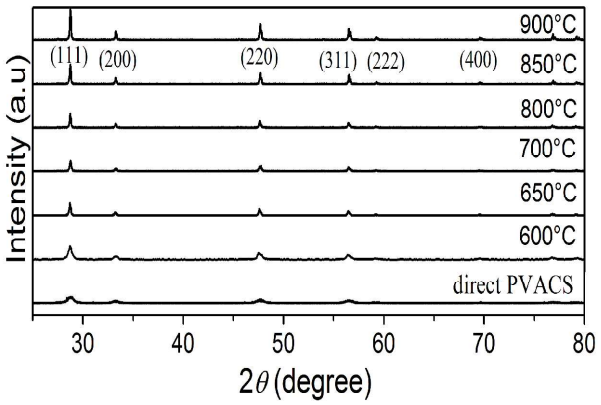

Fig. 1 XRD patterns of CeO_2:Sm^{3+} samples prepared by direct PVACS and a subsequent sintering process from 600 to 900 ^oC.

The samples prepared by PVACS are characterized with XRD patterns to identify their structures. No matter they are heat-treated or not, all the diffraction peaks of the samples are consistent with F-type cubic fluorite structure of CeO_2 (space group: *Fm3m*; JCPDS No.01-081-0792), and no dopant peaks are observed. Figure 1 shows the XRD patterns of $Ce_{1-x}Sm_xO_{2-x/2}$ (x =1.5 mol%) samples prepared by PVACS and a subsequent sintering process. The peaks for all the samples at 28.7^o, 33.3^o, 47.7^o, 56.5^o, 59.3^o and 69.7^o correspond to the (111), (200), (220), (311), (222) and (400) planes, respectively. The results imply the formation of solid solutions through the combustion reaction even without a post-heat-treatment. However, after a subsequent sintering process, the diffraction peaks are obviously higher than those by direct PVACS. Moreover, with the increase of the sintering temperature from 600 to 900 ^oC, the diffraction peaks also gradually increase, manifesting that the sintering process is beneficial to improve the crystallization of the samples.

To further investigate the structure of $Ce_{1-x}Sm_xO_{2-x/2}$ samples, the Raman spectra were measured and given in Fig. 2. The absence of peak at 375 cm^{-1} (Sm_2O_3 phase) implies that Sm^{3+} ions are inserted into the lattice of CeO_2 host, which is in good agreement with the above XRD analysis. The sharp band at

about 460 cm^{-1} is assigned to the Raman-active F_{2g} mode of ceria,[28,29] and it shifts toward lower frequency (from 460 to 457.3 cm^{-1}) with the increase of Sm^{3+} doping concentration (from 0 to 10 mol%). The decreased vibration frequency is due to the lattice expansion with the introduction of Sm^{3+}, which results from the difference of effective ionic radius for Sm^{3+} ion (1.219 Å) and Ce^{4+} ion (1.11 Å) in 8-fold coordination.[30] The peak around 545 cm^{-1} is ascribed to the oxygen vacancies produced in the host CeO_2,[31] which are able to compensate the reduced positive charge owing to the substitution of Ce^{4+} with Sm^{3+}.

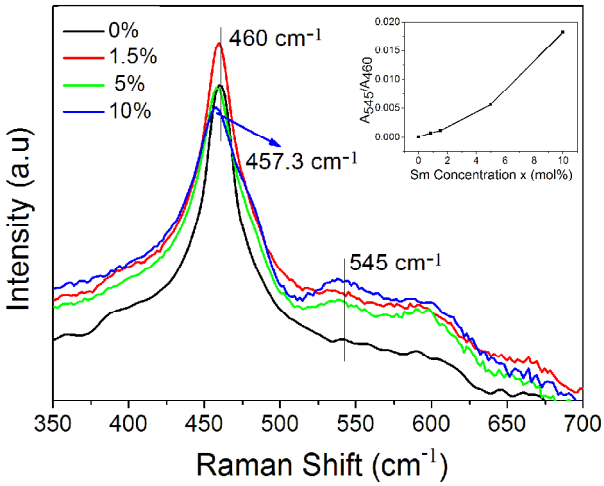

Fig. 2 Raman spectra of CeO_2:Sm^{3+} samples (The inset plots the dependence of A_{545}/A_{460} with Sm doping concentration x).

The dependence of the ratio of peak area of 545 cm^{-1} and 460 cm^{-1} (A_{545}/A_{460}) with Sm^{3+} doping concentration (x) is inset in Fig. 2. It can be seen that the value of A_{545}/A_{460} becomes larger and larger with the increase of Sm^{3+} doping concentration, which suggests the increase of oxygen vacancies content.[34] The creation of oxygen vacancies distorts the cubic lattice of the host, which is certainly to influence the luminescent properties of Sm^{3+} -doped ceria samples.

Fig. 3 displays the SEM photographs of $Ce_{1-x}Sm_xO_{2-x/2}$ (x = 1.5 mol%) samples prepared by PVACS and a subsequent sintering process. The particles prepared by direct PVACS are superfine and the particle size is around 10 nm (Fig. 3a). After a sintering process, most particles are well-dispersed and exhibit clearly round morphology (Fig. 3b-h). The particle size of the samples is closely related with the heat-treatment temperature. With the increase of the heat-treatment temperature from 600 to 900 °C, the particle size is gradually expanded from 30 to about 250 nm, which is in the nano-submicro range.

Nevertheless, for the samples prepared by SCS method, most crystallites are melt together and some micropores can be easily observed (Fig. 4a), which is similar with the previous reported.[24] Even after a sintering duration at 850 °C for 2h (SCS + 850 °C), the aggregation is still very serious and the grains are not well-separated (Fig. 4b). In consequence, the grain shape and particle size of the samples prepared with PVACS can be well-controlled by adjusting the post-heat-treatment temperature. In other words, PVA can serve as a template to control the distribution of grains, which leads to the particles are well-separated.[33-35] Further sintering process promotes the grain growth and crystallinity improvement. Without the existence of PVA, most crystal particles in nanoscale range are bound each other, and can not be divided into individual grains by a subsequent heat-treatment process.

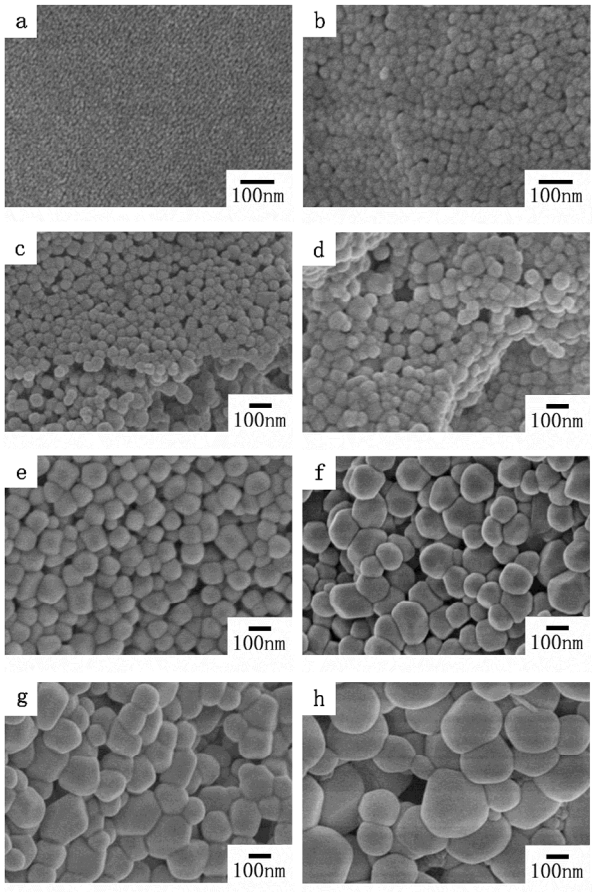

Fig. 3 SEM photographs of CeO_2:Sm^{3+} (x=1.5 mol%) samples prepared by (a) direct PVACS, and subsequent sintering for 2h at (b) 600 °C, (c) 650 °C, (d) 700 °C, (e) 750 °C, (f) 800 °C, (g) 850 °C and (h) 900 °C.

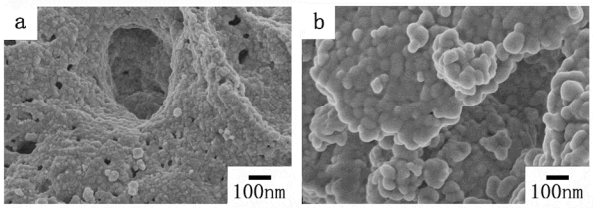

Fig. 4 SEM photographs of CeO_2:Sm^{3+} (x=1.5 mol%) samples prepared by (a) SCS and (b) SCS + 850 °C.

3.2 Luminescent properties.

The photoluminescence spectra of Sm^{3+} -activated CeO_2 samples prepared by PVACS and subsequent heat-treatment at 850 °C (PVACS + 850 °C) are presented in Fig. 5. In the excitation spectra monitored with 622 nm, there is only one broad band from 345 to 420 nm centered at about 370 nm which is assigned to ligand-to-metal CT transition of $O^{2-} \rightarrow Ce^{4+}$ in the host ceria.[6,24,36] The observation of the $O^{2-} \rightarrow Ce^{4+}$ CT band in the excitation spectra of Sm^{3+} -activated ceria demonstrates the energy transfer from host to activator Sm^{3+}. The near-UV excitation range from 345 to 420 nm is quite

suitable to meet the demands of UV LEDs. On the other hand, the emission spectra (excited with 370 nm) consist of some sharp lines corresponding to the characteristic transitions of Sm^{3+} from the $^4G_{5/2}$ level to the ground state $^6H_{5/2}$, and higher levels $^6H_{7/2}$ and $^6H_{9/2}$. Among the emission lines, the magnetic-dipole transitions $^4G_{5/2}\rightarrow{}^6H_{5/2}$ (575 nm) and $^4G_{5/2}\rightarrow{}^6H_{7/2}$ (619, 622 nm) are dominant ones, and the electric-dipole $^4G_{5/2}\rightarrow{}^6H_{9/2}$ (661, 675 nm) transition is subordinate. Therefore, the luminescence color of Sm^{3+} in ceria should be situated in the orange-red spectral region. Similar emission peaks and locations have ever been reported previously.[37,38] Additionally, the luminescence intensities of all the emission peaks are gradually enhanced with the Sm^{3+} concentration increasing as the concentration is less than 1.5 mol%. After the Sm^{3+} concentration is more than 1.5 mol%, the luminescence is greatly decreased. Therefore, the quenching concentration of activator Sm^{3+} should be 1.5 mol% in ceria. The reason for concentration quenching is that the distance between dopant Sm^{3+} ions becomes shorter with the concentration of Sm^{3+} increasing, and collision or energy transfer from one luminescence center to another quenching center has happened.

In our previous work, the quenching concentration of Eu^{3+} in nanoceria can reach as high as 16 mol%, and the dominant emission line is $^5D_0\rightarrow{}^7F_2$ electric-dipole transition.[24] The relatively small quenching concentration (1.5 mol%) of Sm^{3+} in comparison with that of Eu^{3+} (16 mol%) in the same host implies that most activator Sm^{3+} ions have occupied in the crystal lattice sites with inversion symmetry due to the existence of fewer oxygen vacancies. In accordance with Blasse's theory, if a rare-earth ion locates in the crystal lattice with inversion symmetry, optical transitions between levels of the $4f^n$ configuration are forbidden as electric-dipole transition. They can occur as magnetic-dipole transitions which obey the selection rule $\Delta J = 0, \pm1$.[19] Therefore, the $^4G_{5/2}\rightarrow{}^6H_{5/2}$ and $^4G_{5/}\rightarrow{}^6H_{7/2}$ magnetic-dipole transitions always play predominant roles in the emission spectra (Figure 5, 6 and 7).

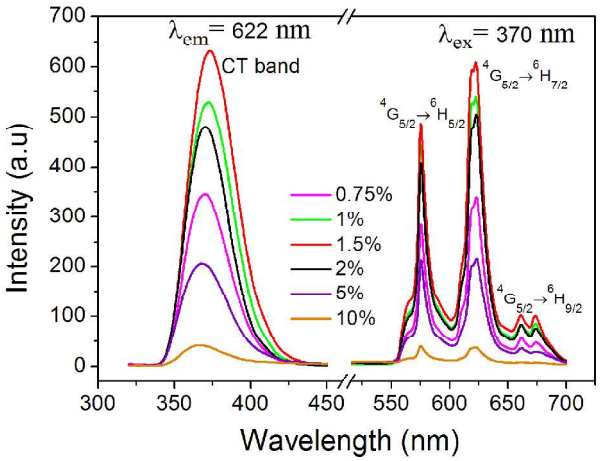

Fig. 5 Excitation (λ_{em}= 622 nm) and emission spectra (λ_{ex}= 370 nm) of $Ce_{1-x}Sm_xO_{2-x/2}$ samples prepared by PVACS + 850 °C.

The luminescence intensity of CeO_2:Sm samples prepared by PVACS is closely related with the subsequent heat-treatment temperature. Fig. 6 shows the photoluminescence of $Ce_{1-x}Sm_xO_{2-x/2}$ (x=1.5 mol%) samples prepared by direct PVACS and post-heat-treatment at different temperatures (from 600 to 900 °C). It is easy to notice that the emission intensity of the sample by PVACS without further heat-treatment is very weak. However, after a subsequent sintering process, the emission intensity is obviously enhanced. For example, if the relative emission intensity is 1 for the sample achieved by direct PVACS, the relative intensity is about three-fold as the sintering temperature is 600 °C (very low sintering temperature), and the relative emission intensity reaches more than 10-fold after the sintering temperature is 800 °C. Further increase of the sintering temperature to 850~900 °C can lead to the relative intensity reach 13-fold. This means that we can control and optimize the luminescence of nano/submicro particles by only adjusting the post-heat-treatment temperature. Under the same Sm^{3+} -doping concentration surroundings, the increase of sintering temperature is a positive factor to enhance the luminescence efficiency. The reason for this is due to the obvious improved crystallization and enlarged particle size after heat-treatment process,[39] as can be confirmed by their XRD patterns (Fig. 1) and SEM photographs (Fig. 3). The improvement of crystallinity makes the activator distribute more evenly in the crystal lattice and the larger particle size results in the less number of the non-radiation relaxation center, and therefore the luminescence intensity is gradually enhanced with the increase of the sintering temperature.

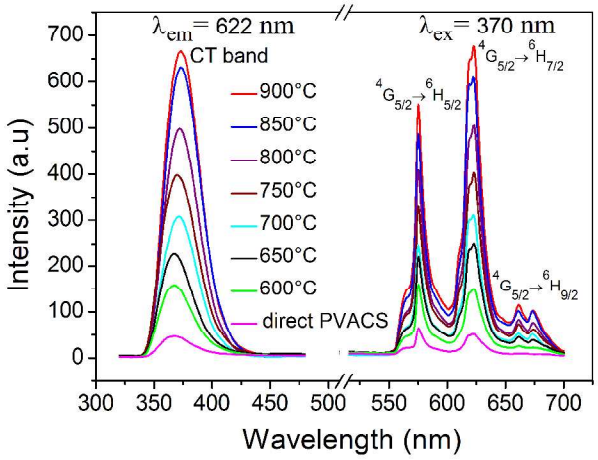

Fig. 6 Photoluminescence of CeO_2:Sm^{3+} (x=1.5 mol%) prepared by direct PVACS and subsequent sintering process at different temperatures for 2h.

However, for the samples prepared by SCS, the emission intensity is not obviously enhanced even after a heat-treatment process at 850 °C for 2h (see Supporting information 1), which may be due to heavy aggregation and almost equal BET surface area after sintering, as can be seen from Fig. 4 and Supporting information 2.

The luminescence intensity and Commission International de L'Eclairage (CIE) chromaticity coordinate of CeO_2:Sm^{3+} (x=1.5 mol%) samples prepared by PVACS + 850 °C , SCS + 850 °C and SSR (1000 °C) methods were compared in Figure 7. Although the spectra range in Fig. 7 is extended from 400 to 700 nm, the luminescence between 400 to 500 nm is neglected to study due to too weak intensity. The luminescence of the sample prepared by conventional SSR is very weak (black curve and image c in Fig. 7) and the relative intensity ratio of transition $^4G_{5/2}\rightarrow{}^6H_{7/2}$ to $^4G_{5/2}\rightarrow{}^6H_{5/2}$ (I_{622} / I_{575}) is almost 1.0. For the sample prepared by SCS + 850 °C, the luminescence intensity (green curve and image b in Fig. 7) is relatively stronger (three-fold) than that by SSR method, and the ratio of I_{622} / I_{575} is increased to 1.2. What the more interesting is that the luminescence intensity of the sample prepared by PVACS +

850 °C is greatly enhanced (red curve and image a in Fig. 7) nearly 10-fold in comparison with that by SSR method, and the ratio of I_{622} / I_{575} is further increased to about1.3. The changed ratio of I_{622} / I_{575} from 1.0 to 1.3 means the increase of red-light content, which is beneficial to tune the emitting-color from orange to red, as can be seen from the CIE chromaticity diagram and images inset of Fig. 7. The detailed CIE chromaticity coordinate values of the above samples have been listed in Table 1.

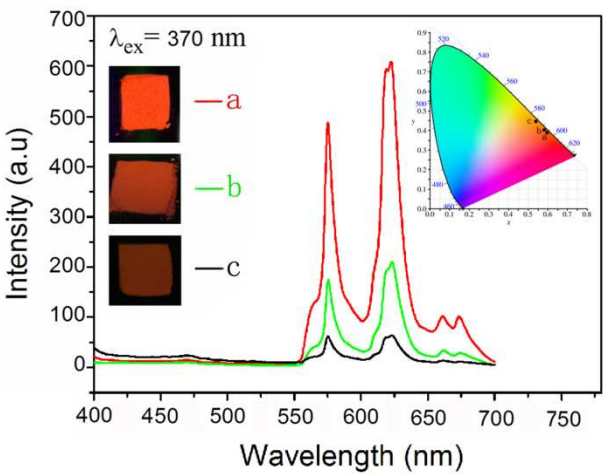

Fig. 7 Emission spectra (λ_{ex}= 370 nm) and corresponding images under a 365 nm UV lamp (left), and CIE chromaticity diagram (upper right) of CeO_2:Sm^{3+} (x=1.5 mol%) prepared by (a) PVACS + 850 °C, (b) SCS + 850 °C, and (c) conventional SSR at 1000 °C for 2h.

The luminescence quantum yields of the above samples were measured at the excitation of 370 nm. Owing to very weak luminescence for the sample prepared by SSR, its quantum yield value is only 0.65%. With the luminescence enhancement of the samples prepared by SCS + 850 °C and PVACS + 850 °C, the quantum yield value is greatly increased to 6.3 and 27.4%, respectively. It is evidently that the quantum yield value depends upon the synthesis condition, and the high quantum yield can be obtained through PVACS and subsequent sintering process. The quantum yields are affected by the probability of the non-radiative transition process, which is responsible for the poor crystallinity and surface defects of the samples.[40] Due to perfect crystallization and smaller specific surface area, the sample prepared by PVACS + 850 °C has a higher quantum yield than that prepared by SCS + 850 °C. It is believed that the quantum yields can be further enhanced by increasing the sintering temperature and duration time.

Time-resolved studies are helpful in exploring the nature of the luminescence and its time dependence, and the fluorescence lifetime of phosphor particles applied in displays and lightings should be appropriate to avoid the overlap of images and signals.[41] Fig. 8 depicts the luminescence decay curves of CeO_2:Sm^{3+} (x=1.5 mol%) samples prepared by direct PVACS, PVACS + 650 °C, and PVACS + 850 °C. All the decay traces can be well-fitted with a double exponential function which is given in equation (1),

$$I = A_1 \times \exp(-t/\tau_1) + A_2 \times \exp(-t/\tau_2) \quad (1)$$

where I is the luminescence intensity at time t, τ_1 and τ_2 are the decay time, A_1 and A_2 are constants. The decay curves with double exponential mean the existence of two luminescence centers in the host. Due to the interface effects of nanoscale materials (the BET specific surface area of CeO_2:Sm^{3+} (x=1.5 mol%) prepared by PVACS and SCS can be found in Supporting information 2), the rate of non-radiative transitions of surface particles should be evidently larger than that of internal particles. In consequence, the lifetime of radiative transition of activator Sm^{3+} on the surface (τ_2) is much lower than that in body site (τ_1), as can be seen from Table 1.

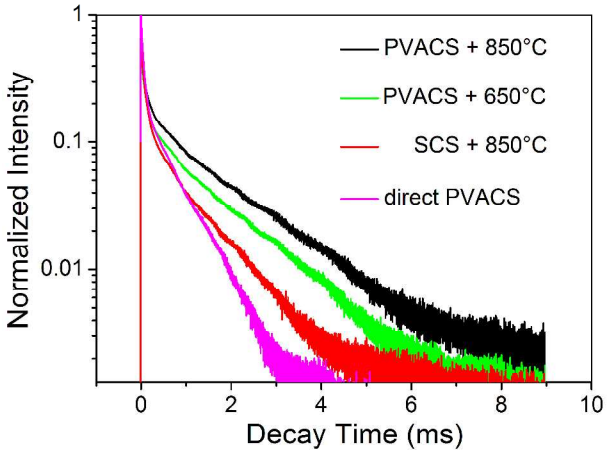

Fig. 8 Luminescence decay curves of CeO_2:Sm^{3+} (x=1.5 mol%) prepared by direct PVACS, PVACS + 650 °C, PVACS + 850 °C and SCS +850 °C.

Additionally, the average lifetimes (τ) have been calculated using the formula (2) and listed in Table 1.[42]

$$\tau = (A_1 \times \tau_1^2 + A_2 \times \tau_2^2) / (A_1 \times \tau_1 + A_2 \times \tau_1) \quad (2)$$

Owing to the smallest particle size and largest specific surface area, the sample prepared with direct PVACS is certainly to produce intense surface effect. As a result, the heavy non-radiative transition of the surface particles leads to the shortest lifetime τ (0.48 ms) among all the samples. After a sintering at 650 and 850 °C, the samples shows relatively larger particle size and smaller specific surface area, and therefore the obviously increased lifetime τ (1.00 and 1.25 ms) is obtained.

Table 1. CIE coordinates and Luminescence lifetime of CeO_2:Sm^{3+} (x=1.5 mol%) prepared by different approaches.

Preparation Approach	CIE Coordinates		Luminescence Lifetime (ms)		
	X	Y	τ_1	τ_2 (%)[a]	τ
PVACS			0.597	0.046 (21.8)	0.48
PVACS +650°C			1.133	0.050 (11.6)	1.00
PVACS +850°C	0.594	0.406	1.365	0.054 (8.9)	1.25
SCS +850 °C	0.585	0.413	0.734	0.045 (17.9)	0.61
SSR 1000°C	0.543	0.453			

[a] percentage of surface luminescent center.

The luminescence lifetime of the sample prepared by SCS + 850 °C is also measured. Without the assistance of PVA as a template, the luminescence of Sm^{3+} in ceria is not strong even

after a heat-treatment process. The luminescence decay trace is also fitted with a double exponential function. This implies that the surface effect in the host can not be neglected although most crystal particles are not separated into individual grains. The fact that relatively shorter lifetime τ (0.61 ms) as compared with that prepared by PVACS + 850 ^{o}C manifests that PVA in CeO_2:Sm^{3+} particles can promote the enhancement not only the luminescence intensity and quantum yield, but also the lifetime.

4. Conclusions

A series of $Ce_{1-x}Sm_xO_{2-x/2}$ (x = 0-10 mol%) nano/submicro particles (10 ~ 250 nm) have been prepared by PVACS and SCS approaches. The XRD and Raman spectra data indicate that Sm^{3+} ions are effectively incorporated into the lattice of ceria and oxygen vacancies are created. Under the excitation of 370 nm originating from $O^{2-}\rightarrow Ce^{4+}$ CT band, the samples emit orange-red light which is attributed to the magnetic-dipole transitions $^4G_{5/2}\rightarrow{}^6H_{5/2}$ (575 nm) and $^4G_{5/2}\rightarrow{}^6H_{7/2}$ (619, 622 nm). The quenching concentration of Sm^{3+} is 1.5 mol%. Applying PVACS approach, not only the morphology of particles is uniform, but also the particle size is obtained from nano (10 nm) to submicro (~250 nm) by simply adjusting the subsequent sintering temperature. The more interesting is that the luminescence intensity of the CeO_2:Sm^{3+} particles can be controlled by increasing the sintering temperature, and the optimal luminescence intensity presents nearly 10-fold in comparison with that of samples prepared by traditional SSR. On the other hand, the samples prepared by SCS does not exhibit well-distributed shape, and the luminescence intensity is very weak. Even after a heat-treatment process at 850 ^{o}C, the aggregation is still very heavy and the luminescence is hardly improved. It can be concluded that PVA as a template plays an indispensable role in limiting the agglomeration of particles, controlling the size of crystal particles and luminescent efficiency of the samples. The suitable excitation wavelength, regular shape and strong luminescence will make CeO_2:Sm^{3+} samples become superior candidates in UV LEDs.

Acknowledgements

We would like to acknowledge the support from the National Nature Science Foundation of China through Grant No. 20971035, the Natural Science Foundation of Hebei Province (China) through Grant No. B201000370, No. 08B012 and the Science Foundation of Hebei Education Department (China) through Grant No.2009136. Wei Chen would like to acknowledge the support from the U.S. Army Medical Research Acquisition Activity (USAMRAA) under Contracts of W81XWH-10-1-0279 and W81XWH-10-1-0234 and partially the NSF and DHS joint ARI program (2011-DN-077-ARI053-02, 3&4).

Notes and references

[a]*College of Chemistry and Materials Science, Hebei Normal University, Shijiazhuang 050024, P. R. China. E-mail: ssk02@mails.tsinghua.edu.cn. Tel: +86-311-80787402. Fax: +86-311-80787402.*

[b]*Analysis Center, Department of Chemistry, Tsinghua University, Beijing 100084, P. R. China.*

[c]*Department of Physics, The University of Texas at Arlington, Arlington, Texas 76019-0059, USA.*

† Electronic Supplementary Information (ESI) available:[The emission spectra of CeO_2:Sm^{3+} (x=1.5 mol%) prepared by SCS, and the BET specific surface area of CeO_2:Sm^{3+} (x=1.5 mol%) sample prepared by SCS and PVACS are given in supplementary information 1 and 2, respectively]. See DOI: 10.1039/b000000x/

1 M. Fernández-García, A. Martínez-Arias, J. C. Hanson and J. A. Rodriguez, *Chem. Rev.*, 2004, **104**, 4063.
2 A. S. Karakoti, S. V. N. T. Kuchibhatla, K. S. Babu and S. Seal, *J. Phys. Chem. C*, 2007, **111**, 17232.
3 S. Babu, J. H. Cho, J. M. Dowding, E. Heckert, C. Komanski, S. Das, J. Colon, C. H. Baker, M. Bass, W. T. Self and S. Seal, *Chem. Commun.*, 2010, **46**, 6915.
4 B. K. Pierscionek, J. Keenan, A. A. Yasseen, L. M. Colhoun, Y. B. Li, R. A, Schachar and W. Chen, *Curr. Anal. Chem.*, 2010, **6**, 172.
5 B. K. Pierscionek, Y. B. Li, A. A. Yasseen, L. M. Colhoun, R. A, Schachar and W. Chen, *Nanotechnology*, 2010, **21**, 035102.
6 W. Y. Hernández, M. A. Centeno, F. Romero-Sarria and J. A. Odriozola, *J. Phys. Chem. C*, 2009, **113**, 5629.
7 Z. Wang, Q. Wang, Y. C. Liao, G. L. Shen, X. Z. Gong, N. Han, H. D. Liu and Y. F. Chen, *ChemPhysChem*, 2011, **12**, 2763.
8 R. V. Mangalaraja, S. Ananthakumar, M. Paulraj, H. Pesenti, M. Lopez, C. P. Camurri, L. A. Barcos and R. E. Avila, *J. Alloys Compd.*, 2012, **510**, 134.
9 S. Park, J. M. Vohs and R. J. Gorte, *Nature*, 2000, **404**, 265.
10 S. Tsunekawa, T. Fukuda and A. Kasuya, *J. Appl. Phys.*, 2000, **87**, 1318.
11 K. Kuntaiah, P. Sudarsanam, B. M. Redd and A. Vinu, *RSC Adv.*, 2013, **3**, 7953.
12 K. Yamashita, K.V. Ramanujachary and M. Greenblatt, *Solid State Ionics*, 1995, **81**, 53.
13 Q. Liu, F. Zhao, X. H. Dong, C. H. Yang and F. L. Chen, *J. Phys. Chem. C*, 2009, **113**, 17262.
14 S. Fujihara and M. Oikawa, *J. Appl. Phys.*, 2004, **95**, 8002.
15 Q. Dai, M. E. Foley, C. J. Breshike, A. Lita and G. F. Strouse, *J. Am. Chem. Soc.*, 2011, **133**, 15475.
16 T. Ninjbadgar, G. Garnweitner, A. Borger, L. M. Goldenberg, O. V. Sakhno and J. Stumpe, *Adv. Funct. Mater.*, 2009, **19**, 1819.
17 Z. H. Xu and J. Lin, *Rev. Nanosci. Nanotechnol.*, 2013, **2**, 225.
18 S. Sandoval, J. Yang, J. G. Alfaro, A. Liberman, M. Makale, C. E. Chiang, I. K. Schuller, A. C. Kummel and W. C. Trogler, *Chem. Mater.*, 2012, **24**, 4222.
19 G. Blasse and B. C. Grabmaier, *Luminescent Materials*, Springer-Verlag, Berlin, 1994, P40.
20 C. Y. Shang, X. Q. Wang, H. Kang and D. M. Han, *J. Appl. Phys.*, 2011, **109**, 104309.
21 Y. Tao, G. W. Zhao, W. P. Zhang and S. D. Xia, *Mater. Res. Bull.*, 1997, **32**, 501.
22 Y. G. Su, L. P. Li and G. S. Li, *Chem. Mater.*, 2008, **20**, 6060.
23 S. K. Shi, J. Gao and J. Zhou, *Opt. Mater.*, 2008, **30**, 1616.
24 S. K. Shi, M. Hossu, R. Hall and W. Chen, *J. Mater. Chem.*, 2012, **22**, 23461.
25 H. A. Höppe, *Angew. Chem. Int. Ed.*, 2009, **48**, 3572.
26 Z. G. Xia, Y. Y. Zhang, M. S. Molokeev, V. V. Atuchin and Y. Luo, *Sci. Rep.*, 2013, **3**, 3310.
27 J. Y. Han, W. B. Im, G. Y. Lee and D. Y. Jeon, *J. Mater. Chem.*, 2012, **22**, 8793.

28 I. Kosacki, T. Suzuki, H. U. Anderson and P. Colomban, *Solid State Ionics*, 2002, **149**, 99.
29 J. R. McBride, K. C. Hass, B. D. Poindexter and W. H. Weber, *J. Appl. Phys.*, 1994, **76**, 2435.
30 R. D. Shannon, *J. Acta Cryst.*, 1976, **A32**, 751.
31 Z. D. Dohcevic-Mitrovic, M. J. Scepanovic, M. U. Grujic-Brojcin, Z. V. Popovic, S. B. Boskovic, B. M. Matovic, M. V Zinkevich and F. Aldinger, *Solid State Commun.,* 2006, **137**, 387.
32 Z. Y. Pu, J. Q. Lu, M. F. Luo and Y. L. Xie, *J. Phys. Chem.* C, 2007, **111**, 18695.
33 J. Dhanaraj, R. Jagannathan, T. R. N. Kutty and C. H. Lu, *J. Phys. Chem. B*, 2001, **105**, 11098.
34 M. Taguchi, S. Takami, T. Adschiri, T. Nakane, K. Sato and T. Naka, *Cryst EngComm.*, 2011, **13**, 2841.
35 B. Yan and W. G. Zhao, *J. Mater. Sci. Eng.,* 2004, **110**, 23.
36 Y. W. Zhang, R. Si, C. S. Liao, C. H.Yan, C. X. Xiao and Y. Kou, *J. Phys. Chem. B,* 2003, **107**, 1015.
37 E. C. C. Souza, H. F. Brito and E. N. S. Muccillo, *J. Alloys Compd.,* 2010, **491**, 460.
38 Z. G. Xia and D. M. Chen, *J. Am. Ceram. Soc.*, 2010, **93**, 1397.
39 S. K. Shi, H. L. Gong, J. J. Wu, M. Luo and J. Zhou, *J. Am. Ceram. Soc.*, 2012, **95**, 3878.
40 K. Inoue, N. Hirosaki, R. J. Xie and T. Takeda, *J. Phys. Chem. C,* 2009, **113**, 9392.
41 J. Zhou, Z. G. Xia, M. X. Yang and K. J. Shen, *J. Mater. Chem.*, 2012, **22**, 21935.
42 S. Murakami, M. Herren, D. Rau and M. Morita, *J. Inorganica Chimica Acta.*, 2000, **300**, 1014.